Integrated physical and numerical simulations of weld seam formation during extrusion of magnesium alloy

Bai, Sheng wen; Fang, Gang; Zhou, Jie

DOI
10.1016/j.jmatprotec.2018.10.025

Publication date
2019

Document Version
Accepted author manuscript

Published in
Journal of Materials Processing Technology

Accepted Manuscript

Title: Integrated Physical and Numerical Simulations of Weld Seam Formation during Extrusion of Magnesium Alloy

Authors: Sheng-wen Bai, Gang Fang, Jie Zhou

PII: S0924-0136(18)30467-9
DOI: https://doi.org/10.1016/j.jmatprotec.2018.10.025
Reference: PROTEC 15978

To appear in: *Journal of Materials Processing Technology*

Received date: 6-2-2018
Revised date: 22-8-2018
Accepted date: 21-10-2018

Please cite this article as: Bai S-wen, Fang G, Zhou J, Integrated Physical and Numerical Simulations of Weld Seam Formation during Extrusion of Magnesium Alloy, *Journal of Materials Processing Tech.* (2018), https://doi.org/10.1016/j.jmatprotec.2018.10.025

Integrated Physical and Numerical Simulations of Weld Seam Formation during Extrusion of Magnesium Alloy

Sheng-wen Bai[1], Gang Fang[1,] *, Jie Zhou [2]

[1] State Key Laboratory of Tribology, Department of Mechanical Engineering, Tsinghua University, Beijing 100084, China

[2] Department of Biomechanical Engineering, Delft University of Technology, Mekelweg 2, 2628 CD Delft, The Netherlands

*Corresponding author, Gang Fang: Tel: +86-10-6278 2694; E-mail: fangg@tsinghua.edu.cn

Graphical abstract

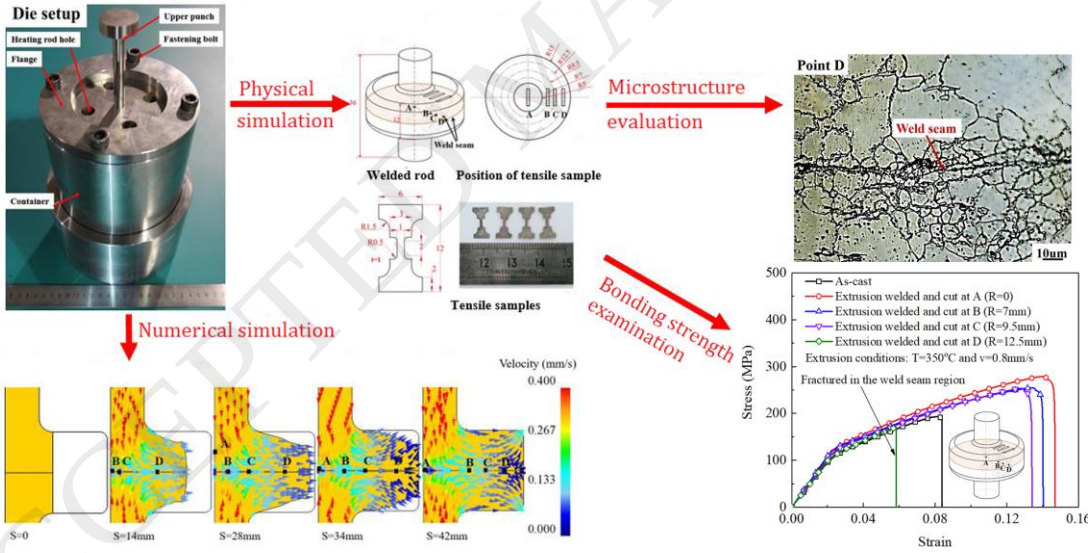

Abstract

Solid-state bonding takes place during the extrusion process to produce a hollow metal profile through a porthole die, known as extrusion welding. Defective weld seams degrade extruded products in mechanical properties. The present research was aimed to determine the effect of extrusion condition on the longitudinal weld seam quality of a magnesium alloy, Mg-8Al-0.5Zn-0.5RE, using an integrated physical and numerical simulation method. A special die set-up for physical simulation was designed, through which two magnesium alloy rods were welded in the solid-state under high hydrostatic pressure. Extrusion welding experiments under different conditions were performed. It was demonstrated that, with this die set-up, the formation of weld seams during extrusion to produce hollow profiles could be physically simulated. The extrusion welding experiments were then numerically simulated to reveal strains, stresses and hydrostatic pressures that could not be experimentally measured. Finally, the tensile strength and elongation of the extrusion-welded magnesium alloy were determined and its microstructure was examined. The results showed that the bonding strength increased with decreasing extrusion speed and rising extrusion temperature. For well-bonded rods, weld seam was invisible under optical microscope. Attributed to high temperature and large equivalent strain, complete dynamic recrystallization occurred across the interface, leading to a reduced average grain size and disappearance of weld seam. By applying the integrated physical and numerical simulation method, extrusion process parameters for a particular magnesium alloy can be optimized to ensure weld seam quality of extruded hollow profiles.

Keywords

Magnesium alloy; Extrusion welding; Weld seam; Solid bonding; Microstructure.

1. Introduction

With increasing requirements for lightweighting of automotive structural parts, magnesium alloys with high strength/weight ratios have been considered to be promising lightweight materials as alternatives to traditional steel and aluminum alloys. At present, most of magnesium alloy products for automotive applications are in the form of castings. Great potential of wrought magnesium alloys with enhanced mechanical performance is yet to be tapped. Forming technologies tailored to the fabrication of magnesium alloy parts are under development. Extrusion is one of the common bulk-forming processes to produce solid, semi-solid or hollow metal profiles, most typically aluminum alloy profiles. Provided that the requirements in mechanical properties for targeted applications are met, hollow profile designs offer great opportunities for weight saving. Hollow profiles are typically produced with porthole dies (Letzig et al., 2008).

During the extrusion process to produce a hollow profile, the billet is forced to be divided into several metal streams at the entrance of a porthole die. These metal streams are then bonded in the welding chamber of the die and finally the bonded billet material flows through the gap between the mandrel and die orifice to form a hollow profile (Donati and Tomesani, 2004). With such a die configuration, weld seams are inevitably present along the whole length of the extruded profile as a result of solid-state bonding occurring inside the welding chamber under high hydrostatic

pressure (Tang et al., 2014a). Weld seams in the extrusion direction are called longitudinal weld seams.

During industrial-scale extrusion in a semi-continuous fashion, the rest of the previously extruded billet remains inside the die after the discard is sheared off and is later on joined by the next billet face to face, resulting in another kind of weld seam, called transverse weld seam (Oosterkamp et al., 2004). Defective longitudinal and transverse weld seams degrade extruded profiles in mechanical performance (Liu et al., 2017). To decrease the uncertainty about weld seam quality of extruded products, especially those for critical load-bearing applications, the section of an extruded profile containing transverse weld seam is usually scraped. However, longitudinal weld seams remain. It is therefore of particular importance to understand the correlation between longitudinal weld seam quality and extrusion conditions, including extrusion temperature, speed and die design.

To gain this understanding, extrusion experiment, numerical simulation and physical simulation have been extensively used in the investigations of longitudinal weld seam quality. Obviously, extrusion experiment is the most straightforward method, but it is practically impossible to get direct access to the welding chamber of the porthole die and thus difficult to gain a full understanding of the mechanisms of extrusion welding. Moreover, with this method, individual effects of extrusion process parameters on longitudinal weld seam quality cannot be studied separately (Bai et al., 2017). Numerical simulation, on the other hand, is a powerful tool to reveal the thermal and mechanical states of the deforming material and thus can be used to improve the understanding of metal flow inside the welding chamber. Lee et al. (2005), for example, studied the effect of porthole die design on extruded aluminum alloy tubes by means of numerical simulation. Khan et al. (2010) made use of a

simplified finite element (FE) model to investigate the metal flow behavior during the extrusion process. Based on the understanding of metal flow from numerical simulation, an extrusion-welding limit diagram was established to predict weld seam quality (Khan et al., 2012). Lu et al. (2016) performed numerical simulation and developed a welding criterion. The parameters used in the welding criterion, such as hydrostatic pressure, equivalent stress and strain rate were drawn from numerically simulated results. However, the numerical simulation method cannot be used to model metallurgical events that take place during solid-state bonding.

It is commonly acknowledged that neither extrusion experiment nor numerical simulation can fulfil the need for a thorough investigation into extrusion welding. A combination of these two methods can however overcome most of the disadvantages of each of the methods. Yu et al. (2016a), for example, studied the extrusion welding of an aluminum alloy using the method combining extrusion experiment and numerical simulation. Being different from the pressure-time criterion (Plata and Piwnik, 2000) and pressure-time-flow criterion (Donati and Tomesani, 2004) established earlier, a new extrusion welding criterion was proposed, by which the effect of inter-diffusion across the weld seam was considered. Yu et al. (2016b) carried further on to investigate the effect of welding chamber geometry on T-seams (transverse weld seams) and L-seams (longitudinal weld seams) through experiment and numerical simulation. They found that a deep welding chamber could lead to good mechanical properties at L-seams. Some new grains were generated in the welding region, but defects such as micro-voids appeared at weld seam (Yu et al., 2017).

Other researchers also used the combined method of extrusion experiment and numerical simulation to study extrusion welding during the extrusion of magnesium

alloys. Li et al. (2008), for example, investigated the thermomechanical behavior of a magnesium alloy, AZ31, during extrusion to produce square tubes by performing numerical simulations and extrusion experiments. It was suggested that the maximum normal pressure in the welding chamber relative to the flow stress of the deforming material determined the weld seam quality. Liu et al. (2008) used the same method to analyze the effect of ram speed on the weld strength of the same magnesium alloy, AZ31. Temperature rise during extrusion caused by increasing ram speed was found to be the main cause for improved bonding strength at weld seam. Zhang et al. (2017) studied the solid-state bonding behavior of AZ31 during extrusion, including microstructure analysis of the weld seam area and determination of weld strength. They found that the profile extruded at 380 °C had the highest tensile strength and elongation, because of sound weld seam and fine grain sizes. Gensch et al. (2016) found that all weld seams in the extruded profiles of a magnesium alloy, ME21, were structurally sound and recrystallized, fine-grained microstructure dominated the as-extruded microstructure, which confirmed the important contribution of dynamic recrystallization to structural integration across the weld seam. In addition, manganese-containing particles and $Mg_{12}Ce$ particles were distributed in the weld seam area. Alharthi and Misiolek (2013) investigated the microstructures in the welding region of the magnesium alloy, AM30. They tried to correlate the ratio of the normal pressure to effective stress (P_n/σ) with extrusion condition by means of numerical modeling (Alharthi et al. 2014).

Compared with the complex variables in extrusion experiment with porthole die, the parameters in physical simulation are easier to control. In other words, by applying physical simulation, the effects of individual process parameters on weld seam quality can be investigated separately. The method combining physical and

numerical simulations is an effective way to study extrusion welding. Edwards et al. (2006a), for example, physically simulated extrusion welding by performing face-to-face compression of two cylindrical rods of an aluminum alloy, AA7020. They determined the weld seam quality by performing tensile tests of bonded rods. Strain, strain rate, rod length and deformation time were considered to be the parameters of interest that could influence bonding quality. The bulge at the bonding interface, generated during compression and corresponding to strain, was taken as an index correlated to the bonding quality. In addition to the strain at the bonding interface, a sufficiently long bonding time was considered important for bonding quality. The same method was applied to investigate the extrusion welding of the AA6082 alloy and similar conclusions were drawn (Edwards et al., 2006b). This method was also employed by Tang et al. in their research on the extrusion welding of the AA3003 alloy (Tang et al., 2014b). They concluded that the bonding strength could reach eighty percent of the strength of the parent material, if the pressure at the welding interface was larger than 87 MPa. Bariani et al. (2006) developed a new method of physical simulation and compressed a cylindrical billet of the AA6060 aluminum alloy with a steel pin inserted. The billet was forced to split around the steel pin and the newly created surfaces then merged to form a weld seam under hydrostatic pressure. With this method, the effects of extrusion process parameters on extrusion welding could be investigated individually. However, all these physical simulations performed in the open environment did not really represent the actual condition inside the welding chamber, because in real extrusion through a porthole die, solid-state bonding occurs under high hydrostatic pressure in a closed welding chamber.

For proper physical simulation of extrusion welding, solid-state bonding should occur in a closed welding chamber. Moreover, the metal flow behavior in the physical

simulation should be similar to real extrusion through a hollow profile. To meet the first requirement, Fang et al. (2017) designed a special die for the physical simulation of the extrusion welding of the AA6063 aluminum alloy. A closed welding chamber was indeed able to create high hydrostatic pressure inside, which was needed for extrusion welding. Bai et al. (2017) modified the die design and investigated the extrusion welding of the AA6082 aluminum alloy. The solid-state bonding strength and microstructure evolution of the alloy during physical simulation were analyzed. In their physical simulations, deformation parameters could be separately controlled to reveal their effects on weld seam quality. However, there were some shortcomings in the previous physical simulations. The aluminum alloy flowed into the welding chamber in the form of "head to head", which did not reflect the characteristic metal flow in a porthole die. In addition, the welding chamber of the die was rather small (12 mm in diameter), which restricted metal flow. It was therefore necessary to develop the physical simulation method further to satisfy the welding condition as that occurring during real extrusion.

It should be noted that during real extrusion through a porthole die, the solid-state bonding of metal streams occurs in an oxide-free environment and the fresh surfaces of split metal streams without any oxide contamination become bonded in the welding chamber to form weld seams. In the physical simulation of extrusion, however, the surfaces of the billet inevitably become oxidized prior to bonding, and oxide contamination may influence the bonding of these two surfaces and thus the quality of the weld seam. Therefore, it is necessary to minimize oxide contamination by e.g., polishing the surfaces just before extrusion welding.

Up till now, there has been little research by means of physical simulation to gain a thorough understanding of the effect of extrusion condition on the weld seam

quality of magnesium alloys. The conclusions drawn from the investigations of aluminum alloys cannot be used directly to predict the weld seam quality of extruded magnesium alloys, because deformation and solid-state bonding behaviors of the two alloy families are distinctly different. Compared with aluminum alloys, for example, dynamic recrystallization (DRX) is easier to be triggered to occur in the case of magnesium alloys, due to a lack of easily activated slip systems even at a sufficiently elevated temperature (Ebrahimi et al., 2011). In addition, the oxide film in the welding interface of magnesium alloy is easier to break up than that on aluminum alloy (You et al., 2000). These factors cause the differences in solid-state bonding behavior between magnesium alloys and aluminum alloys. Therefore, it is of important significance to develop an effective method combining physical and numerical simulations to study the extrusion welding characteristics of magnesium alloys.

To investigate the effects of extrusion parameters on weld seam quality and to gain a comprehensive understanding of the extrusion welding of magnesium alloys, a new die set-up for physical simulation was developed to imitate the real condition of metal flow and bonding in extrusion welding. With this die set-up, two cylindrical rods of a magnesium alloy were extruded into a closed welding chamber and then became solid-state bonded under high hydrostatic pressure. Extrusion welding experiments at different temperatures and extrusion speeds were conducted. FE simulations corresponding to the extrusion welding experiments were performed to calculate the stresses, strains and temperatures of the deforming metal. To evaluate weld seam quality at different extrusion conditions, tensile tests and microstructure analysis of solid-state bonded magnesium alloy rods were performed.

2. Physical simulation experiments

2.1 Die set-up used to model extrusion welding

To overcome the shortcomings of the die set-up for the physical simulation of extrusion welding in the precious research (Bai et al., 2017), in the present research, a modified die set-up was designed for the extrusion welding of two magnesium alloy rods. With this modified die set-up, magnesium alloy rods could be solid-state bonded inside an imitative welding chamber in an environment close to that in real extrusion through a porthole die. Fig. 1 compares the designs of the previous die set-up and the present die set-up and resultant metal flow characteristics inside the welding chamber. The present die set-up was improved in the following three aspects: the control of metal flow, the design of the welding chamber and heating condition.

During the physical simulation of extrusion welding through the previous die set-up (Fig. 1a and b), the upper rod is pushed downwards and becomes bonded to the fixed lower rod under high hydrostatic pressure in the welding chamber. In this way, the displacements of the upper rod and lower rod are not symmetrical with respect to the welding interface (weld seam), which deviates from the joining of two metal streams inside a typical porthole die. Strains and strain rates distributed in these two rods are quite different; the upper rod undergoes more severe deformation than the lower rod. Consequently, the weld seam appears to be umbrella-shaped and thus the longitudinal welding condition during the extrusion of hollow profiles is not best represented (Fig. 1b).

In the present research, the die set-up for the physical simulation of extrusion welding was modified. The essential modification of the die lies the welding chamber that can move relative to the fixed lower rod (Fig. 1c and d). In this way, the metal of

the upper and lower rods deforms symmetrically on both sides of the welding interface (Fig. 1d). To realize the downward movement of the die, a positioning shoulder is placed near the head of the rod (Fig. 2) in contact with the welding chamber wall. During extrusion welding, the upper rod is pushed downwards by the upper punch, while the lower rod is constrained by the lower punch in the axial direction. In this way, due to the action of the shoulder of the lower rod, the interface between these two rods (i.e., the welding interface) is also pushed downwards together with the die. As a result, the upper and lower rods are extruded into the welding chamber symmetrically (Fig. 1d). Then, these two rods become bonded together under high hydrostatic pressure. The split die is placed in a conical container so that bonded rods can be easily taken out. The whole die set-up can be mounted on a universal testing machine or on a hydraulic press whose crosshead speed can be precisely controlled. In the present work, the extrusion welding experiments were performed on a hydraulic press with a force capacity of 2 MN.

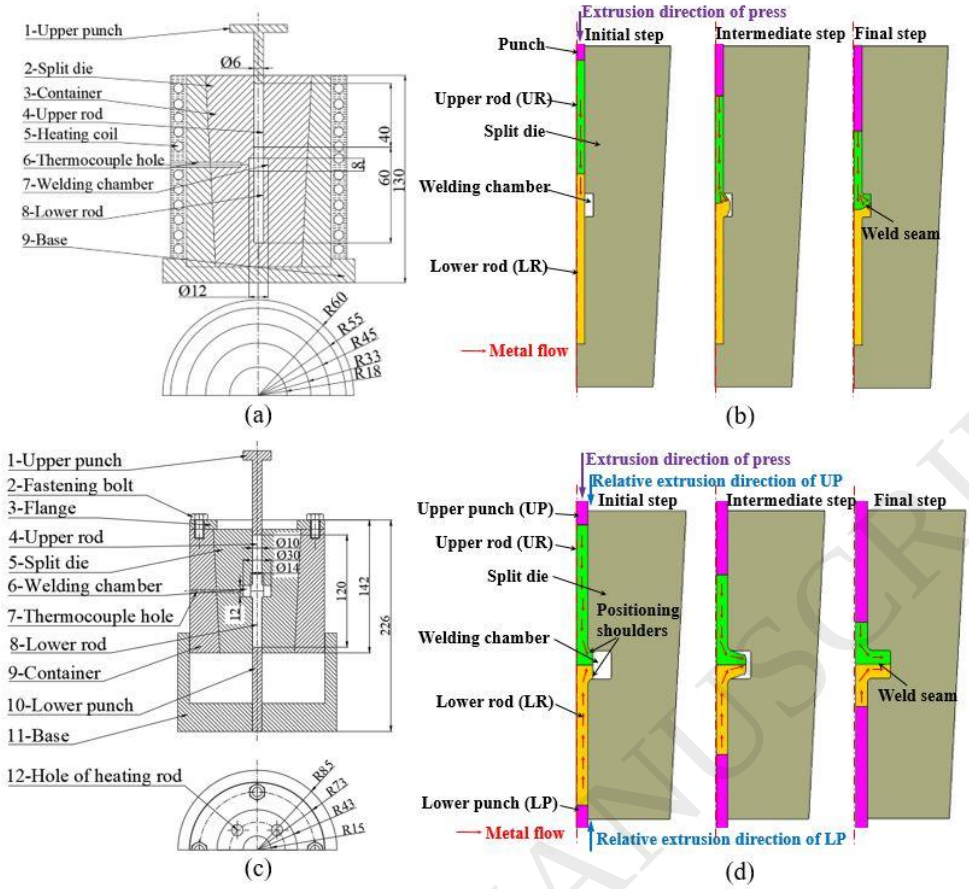

Fig. 1 Schematics of one half of (a) the previously used die set-up and (c) the modified (present) die set-up and metal flow through (b) the previous die set-up and (d) the present die set-up.

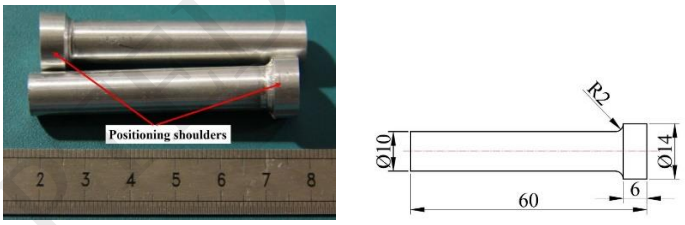

(a) (b)

Fig. 2 Magnesium alloy rods with positioning shoulders used in the present physical simulations of extrusion welding (a) and the dimensions of the rod (b).

In the present die set-up, four heating rods inserted into the die were used to heat the die directly, instead of heating coil around the die in the previous die set-up design. Magnesium alloy rods were contained in the die and synchronously heated. The integral heating power was much higher (2400 W) than that of heating coil (1500 W).

Heating time from room temperature to 400 °C could be shortened from 80 to 40 min. A PID (proportional–integral–derivative) controller was used to regulate the temperature of the die by inputting the feedback temperature signal measured at a spot close to the welding chamber. The temperature of heated magnesium alloy rods was monitored by a separate thermocouple.

A larger welding chamber (Ø30×12 mm) was adopted in the present die design, compared to that (Ø12 × 8mm) of the previous die (Bai et al., 2017). It provided larger space for metal streams from the two rods to flow radially (Fig. 1d). Obviously, the present die set-up could better mimic metal flow in the weld seam area of a hollow profile through a porthole. Fig. 3 shows the new die set-up for the physical simulation of extrusion welding.

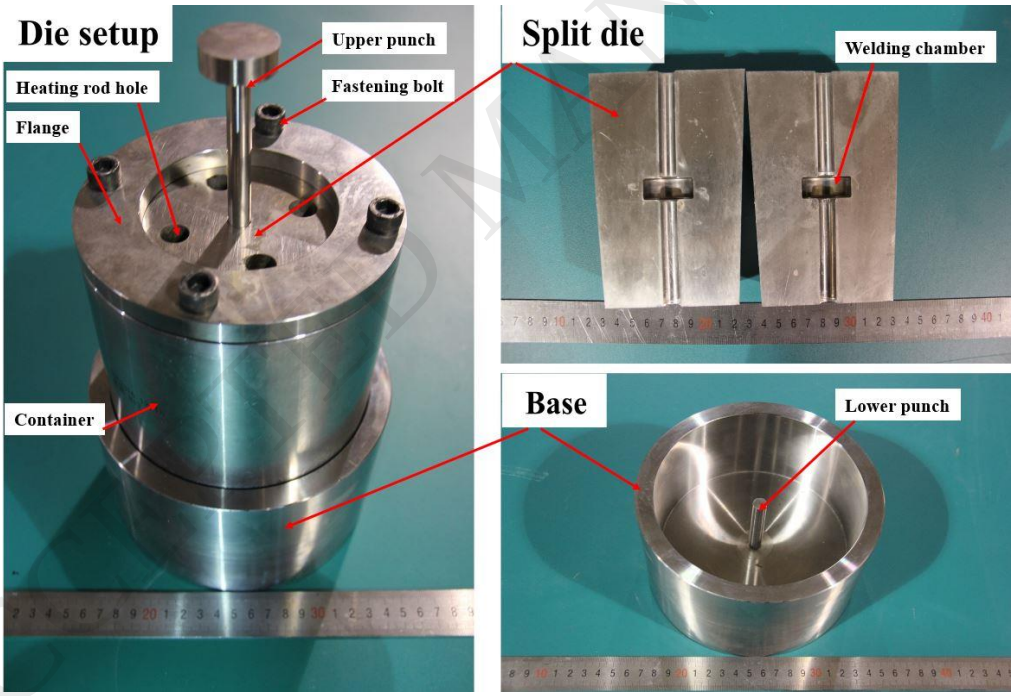

Fig. 3 Die set-up for the physical simulation of extrusion welding.

2.2 Magnesium alloy as billet material

A magnesium alloy containing rare earth elements (Mg-8Al-0.5Zn-0.5RE) was selected for the present research. Table 1 presents the chemical composition of the

magnesium alloy investigated. It possessed better performance in mechanical properties and corrosion resistance, as compared to most of other magnesium alloys. As-cast magnesium alloy billets were subjected to a solid-solution treatment at 420 °C for 24 h and then machined into cylindrical rods with a positioning shoulder near the head (Fig. 2). Each rod of the magnesium alloy had a total length of 60 mm, a body diameter of 10 mm and a head with a diameter of 14 mm and a length of 6 mm. To minimize oxidation occurring to the surfaces that were expected to be bonded, the head face of the billet was polished just before extrusion welding.

Table 1. Chemical composition (wt.%) of the investigated magnesium alloy.

Element	Al	Zn	Mn	La	Gd	Mg
Content (wt.%)	8.0~8.8	0.3~0.8	0.15~0.3	0.7~1.3	0.3~0.7	Bal.

2.3 Extrusion welding experiments

Before the extrusion welding experiments, the interface between the two rods was placed at a vertically symmetric plane of the welding chamber. The die and two rods were heated to a specified temperature at a rate of 10 °C/min and soaked at this temperature for 15 min.

During the experiments, the two rods were axially upset and their heads were then forced to flow radially into the vacant space of the welding chamber and finally solid-state bonding occurred. The ram speed of the hydraulic press used was set at 0.8, 1.4 and 2.0 mm/s, corresponding to the relative speeds of the upper and lower punches at 0.4, 0.7 and 1.0 mm/s relative to the movable split die (Fig. 1d), respectively. The initial temperatures of rods and die were set at 300, 350 and 400 °C. According to the results of previous uniaxial compression tests, the formability of this

alloy was poor at temperatures lower than 300 °C and hot shortness was prone to occur at temperatures higher than 420 °C.

After extrusion welding, the bonded sample together with the die was cooled by spraying water and then immersed in water immediately to freeze the as-deformed microstructure. When the die temperature dropped to near room temperature, the bonded sample was taken out of the split die.

2.4 Tensile test

After the physical simulation experiments, bonded samples with a waist diameter of 30 mm, a body diameter of 10 mm and a height of 36 mm were obtained. Tensile tests of the bonded samples were performed to evaluate the quality of weld seams formed at different conditions, i.e., at different temperatures and extrusion speeds. As schematically shown in Fig. 4, four tensile specimens arrayed in parallel to each other along the axial direction were cut out from a bonded sample at four positions, A, B, C and D, where the radii were 0, 7, 9.5, 12.5 mm, respectively. These positions corresponded to the positions A, B, C and D. Fig. 4d shows the tensile specimens cut out from a welded sample by means of wire electro-discharge machining (EDM).

The dimensional details of the tensile specimens are given in Fig. 4c. The tensile specimen was designed as a notched tensile specimen in order to ensure that fracture would occur at the weld seam of the specimen. In this way, the tensile strength of the specimen would be a measure of the bonding strength.

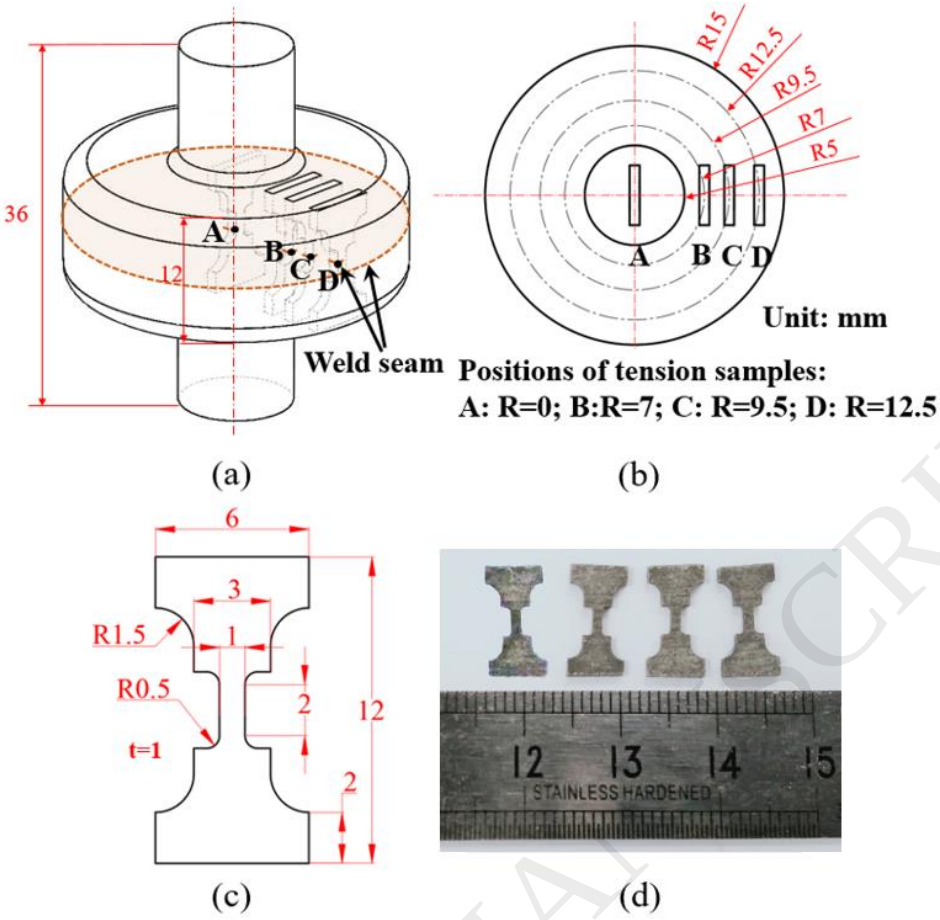

Fig. 4 Preparation of tensile specimens from solid-state bonded rods: (a) schematic of bonded sample; (b) specimen positions; (c) specimen dimensions; (d) tensile specimens with surface speckles.

Tensile tests were conducted on a universal testing machine (AG-X, Shimadzu) and a pair of specially designed clamps were employed (Fig. 5). The same tensile test was repeated twice and the tensile stress-strain curves were obtained. Crosshead speed was set to be 0.5 mm/min.

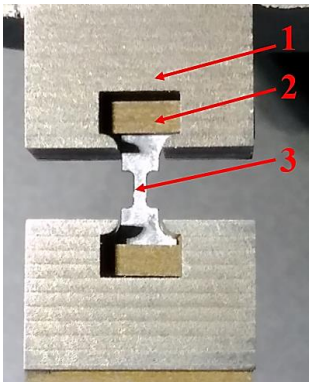

Fig. 5 Tensile specimen clamped by a specially designed tool mounted on a universal testing machine: 1-tensile testing jig; 2-dowel; 3-tensile specimen.

2.5 Microstructural observation

To observe the microstructure of the magnesium alloy in the extrusion welding region, samples were cut at the positions near the tensile specimens, ground and mechanically polished. A solution composed of 4 g picric acid, 25 ml alcohol and 50 ml water was used to etch the samples. Etching time was 30 s. Microstructural examination of the samples was carried out using an optical microscope (Zeiss).

3. Finite element simulations

To analyze the extrusion welding process quantitatively, it is necessary to obtain important mechanical variables, i.e., stress, strain and strain rate of the deforming material inside the welding chamber by means of FE simulation. In addition, through FE simulation, the die set-up designed for physical simulation (section 2.1) could be validated before die manufacturing and tooling preparation.

Considering the symmetry of the die set-up and cylindrical magnesium alloy rods, an axisymmetric FE model corresponding to the physical simulation experiments was built by using commercial FE software DEFORM. The components in the numerical

simulation model included the upper punch, lower punch, two cylindrical magnesium alloy rods and split die. All these components were meshed into quadrilateral elements (Fig. 6).

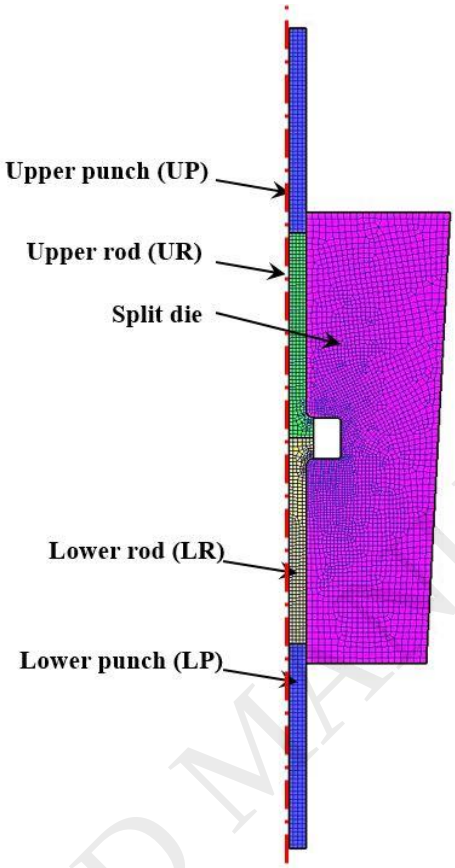

Fig. 6 FE model of extrusion welding.

The geometrical parameters of tooling and rods in the FE model were the same as those used in the physical simulation experiments. The tooling was considered to be rigid (without deformation) and its temperature evolution was incorporated into the model. The thermal properties of the tool steel H13 used for the extrusion tooling were defined, according to the material library of DEFORM 11.0. The rigid-plastic properties of the magnesium alloy were assumed. To describe the plastic deformation behavior of the magnesium alloy, Mg-8Al-0.5Zn-0.5RE, uniaxial compression tests of cylindrical specimens were carried out by using a Gleeble 1500 thermomechanical simulator. The temperatures were set at 300, 330, 360, 390 and 420 °C and the strain

rates were 0.001, 0.01, 0.1, 1 and 10 s^{-1}. The data of true stress and true strain measured from the compression tests were imported into the DEFORM software to establish a constitutive model of the magnesium alloy. The thermal-mechanical coupling effect of magnesium alloy was considered in the FE simulation.

The temperature of the split die was set to be the same as that of magnesium rods, while the initial temperature of the upper punch and lower punch was set at 20 °C. Heat exchanges between the rods, tooling and environment were taken into account in the FE simulations. The thermal properties of the magnesium alloy for the billet and H13 tool steel for the extrusion tooling, used in the FE model, are listed in Table 2 (Liu et al. 2008).

A shear friction model (Tresca model) was used to model the friction between the rods and tooling. The friction factor at the interfaces was set at 1.0 (Li et al., 2008). The extrusion speeds of the upper punch and the lower punch were set at 0.4, 0.7 and 1.0 mm/s.

Table 2. Thermal properties of the workpiece and extrusion welding tooling.

Physical property	Magnesium alloy	H13 tool steel
Thermal conductivity (W/(m °C))	96	28.4
Heat capacity (N/(mm^2 °C))	2.09684 at 327 °C, 2.27484 at 527 °C	5.6
Heat transfer coefficient between tooling and workpiece (N/(°C s mm^2))	11	11
Heat transfer coefficient between tooling/workpiece and air (N/(°C s mm^2))	0.02	0.02
Emissivity	0.7	0.7

4. Results and discussion

4.1. Metal flow and bonding

Fig. 7a and b shows the FE simulated velocity and strain distributions in the deforming rods, respectively, along with increasing punch stroke to 14, 28, 34 and 42 mm. Increasing deformation of the two rods occurred at a temperature of 350 °C and an extrusion speed of 0.8 mm/s. Four points, A, B, C and D at the welding interface, were selected, corresponding to the positions of 0, 7, 9.5 and 12.5 mm in the radial direction at the welding interface of the two rods of the magnesium alloy (Fig. 7), respectively. These marked points were traced by the 'Point Tracing Method' of DEFORM 2D along with increasing punch stroke.

FE simulation results showed that the two rods gradually flowed into the vacant space in the radial direction. The magnesium alloy then flowed into the corners of the welding chamber when the heads of the rods met the inner wall of the welding chamber. Finally, the rods filled the welding chamber completely. Solid-state bonding occurred at the interface between the two rods and the weld seam was located at the symmetrical interface of the upper and lower rods (Fig. 7a).

During the extrusion process, the largest equivalent strain appeared at the welding interface. In addition, large strains occurred in the region near the upper and lower wall of the welding chamber (Fig. 7b). It was the severe friction that resulted in the large strains in these regions. When the extrusion stroke was 42 mm and the welding chamber was filled with the deforming magnesium alloy, a weld seam was formed under high hydrostatic pressure. The final equivalent strains in points A, B, C and D were 4.54, 4.50, 4.79 and 2.54, respectively (Fig. 7b). The confining effect of the welding chamber wall on metal flow led to a relatively low strain at point D.

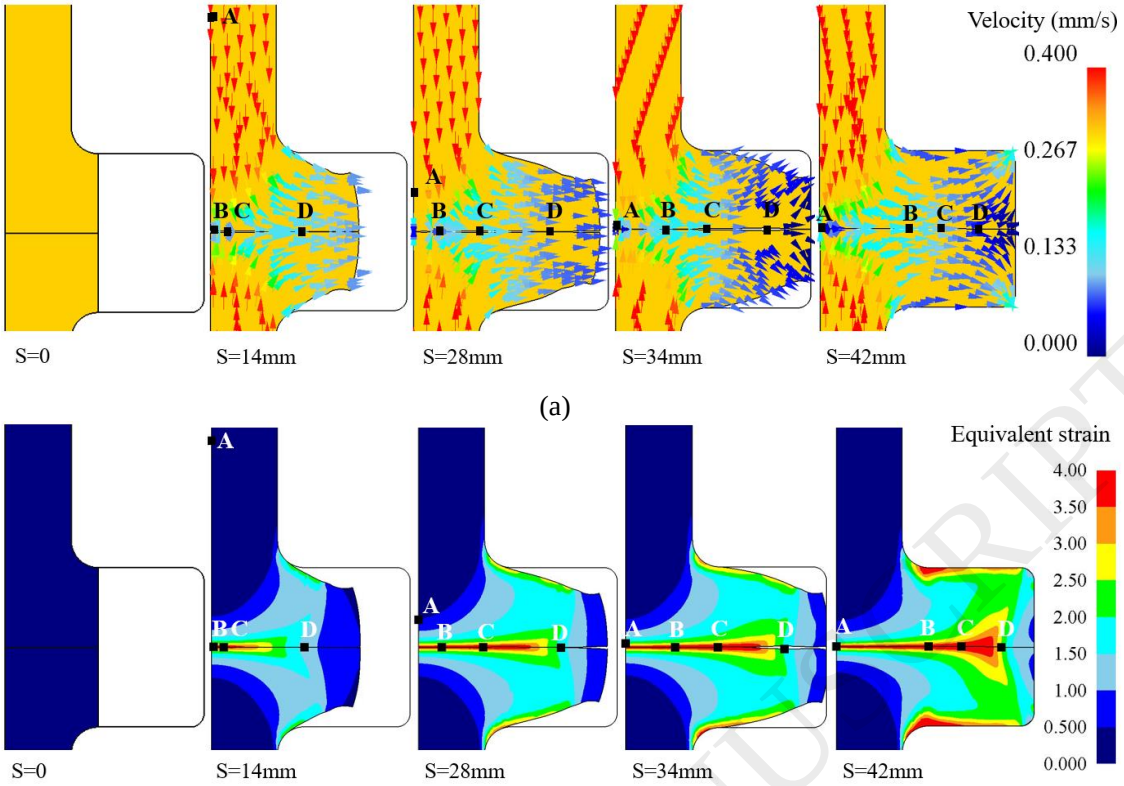

(a)

(b)

Fig. 7 FE simulated results of metal flow in the welding chamber when the extrusion temperature and speed were 350 °C and 0.8 mm/s, respectively: (a) velocity fields and (b) equivalent strain fields.

Fig. 8 shows an extrusion-welded sample. With respect to the sample shape and the position of the weld seam, the FE simulation (Fig. 7b) had a good agreement with the experimental results. The weld seam of the bonded sample was located right in the middle of the welding chamber, which is the main objective of the present die set-up design.

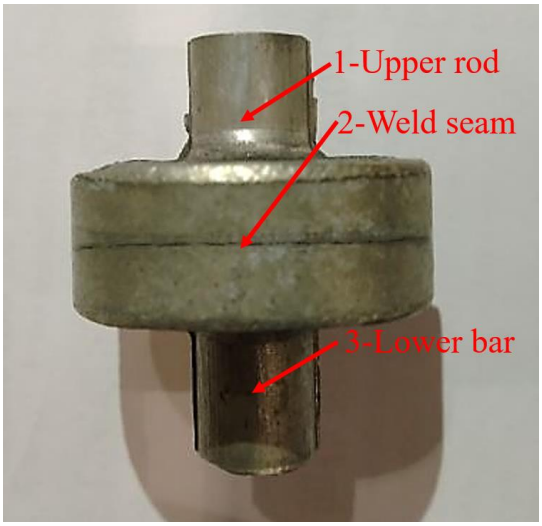

Fig. 8. Extrusion-welded sample at a punch stroke of 42 mm, an extrusion speed of 0.8 mm/s and a temperature of 350 °C.

Fig. 9 shows the variations of measured and simulated temperatures with punch stroke at a point monitored by a thermocouple, which was 5 mm from the welding chamber in the radial direction. The initial temperature of the two rods and die was all 350 °C and the extrusion speed was set at 0.8, 1.4 and 2.0 mm/s. It was observed that the temperature declined during the extrusion process due to heat exchanges between the die set-up and surrounding air. Overall, a higher extrusion speed led to a higher temperature. At extrusion speeds of 0.8, 1.4 and 2.0 mm/s, the measured temperatures at a ram displacement of 42 mm were 337, 343 and 345 °C, respectively, while the corresponding simulated values were 335, 344 and 348 °C, respectively. The differences between the measured and simulated temperatures did not exceed 0.9%.

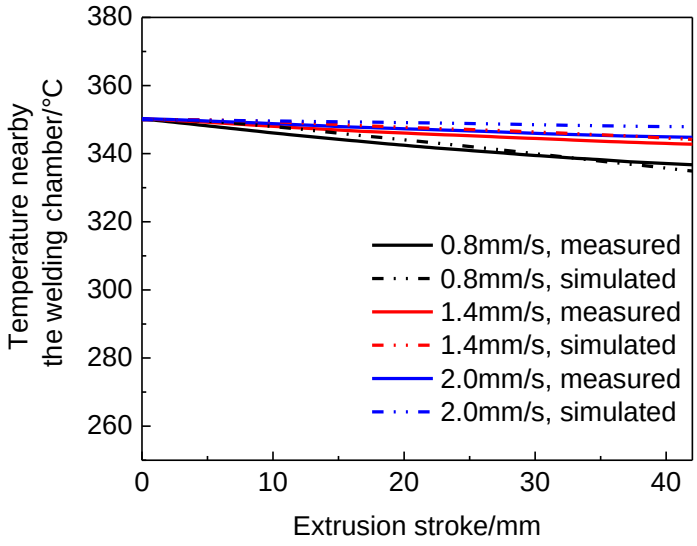

Fig. 9 Temperature evolution at a point monitored by a thermocouple during extrusion welding at an initial temperature of 350 °C and extrusion speeds of 0.8, 1.4 and 2 mm/s.

The distribution of hydrostatic pressure inside the welding chamber was of critical importance for solid-state bonding occurring during extrusion (Bai et al., 2017). Fig. 10 shows the distribution of hydrostatic pressures in the radial direction at the bonding interface when the welding chamber was filled with the magnesium alloy. The corresponding extrusion speed and temperature were 0.8 mm/s and 350 °C, respectively. The hydrostatic pressure in the radial direction inside the welding chamber decreased in a wavy pattern. It reached a valley value (214.1 MPa) and a peak value (233.7 MPa) at points of 9.8 and 13.3 mm, respectively, away from the center. The hydrostatic pressure values at points A, B, C and D were 282.7, 238.9, 214.3 and 229.6 MPa, respectively.

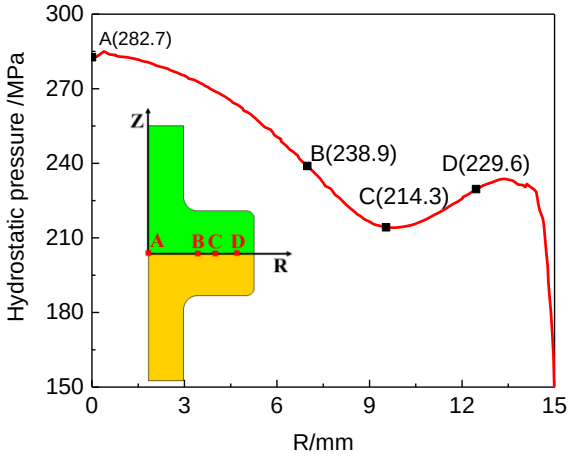

Fig. 10 Distribution of hydrostatic pressures at the welding interface during extrusion welding at an extrusion speed of 0.8 mm/s and a temperature of 350 °C.

Fig. 11 shows the simulated hydrostatic pressure distributions in the rods extruded at different extrusion speeds and at an initial temperature of 350 °C. It can be seen from Fig. 11a that hydrostatic pressure increased with increasing extrusion speed. Fig. 11b shows that hydrostatic pressures at the welding interface were 145.0~285.0 MPa, 156.0~294.3 MPa and 166.8~302.4 MPa, when the extrusion speeds were 0.8, 1.4 and 2.0 mm/s, respectively. The flow stress of the magnesium alloy affected the hydrostatic pressure significantly. A higher extrusion speed led to a higher flow stress of the magnesium alloy (Quan et al., 2011), which in turn led to a higher hydrostatic pressure inside the welding chamber.

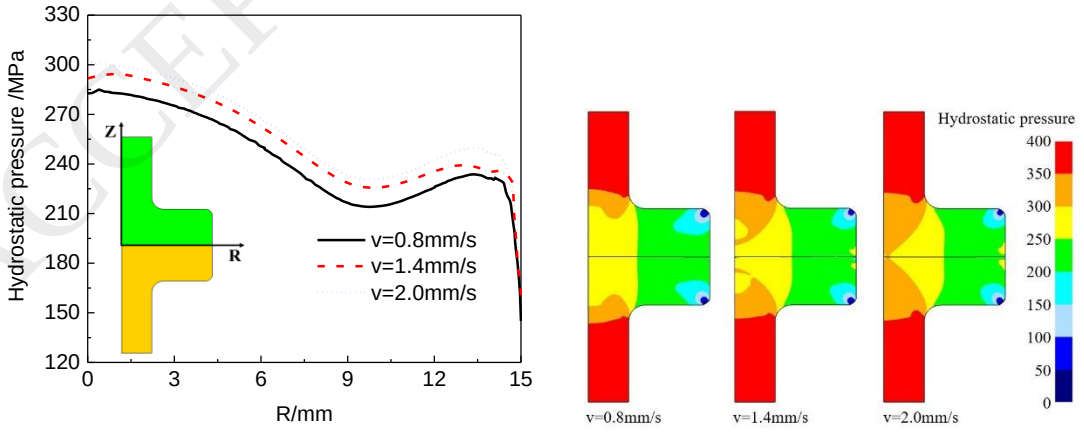

(a) (b)

Fig. 11. FE calculated hydrostatic pressure distributions in the samples extruded at an initial temperature of 350 ℃ and speeds of 0.8, 1.4, 2.0 mm/s: (a) at the welding interface in the radial direction of the die and (b) in the welded samples.

On the other hand, a higher temperature resulted in a lower flow stress of the magnesium alloy during the hot extrusion process. Therefore, the hydrostatic pressure in the welding chamber decreased with increasing temperature (Fig. 12a). When the temperatures were 300, 350 and 400 ℃, the hydrostatic pressures at the welding interface were 164.5~389.1 MPa, 145.0~285.0 MPa and 133.8~220.6 MPa, respectively (Fig. 12b). It could be concluded that the hydrostatic pressure in the welding chamber was quite sensitive to extrusion temperature.

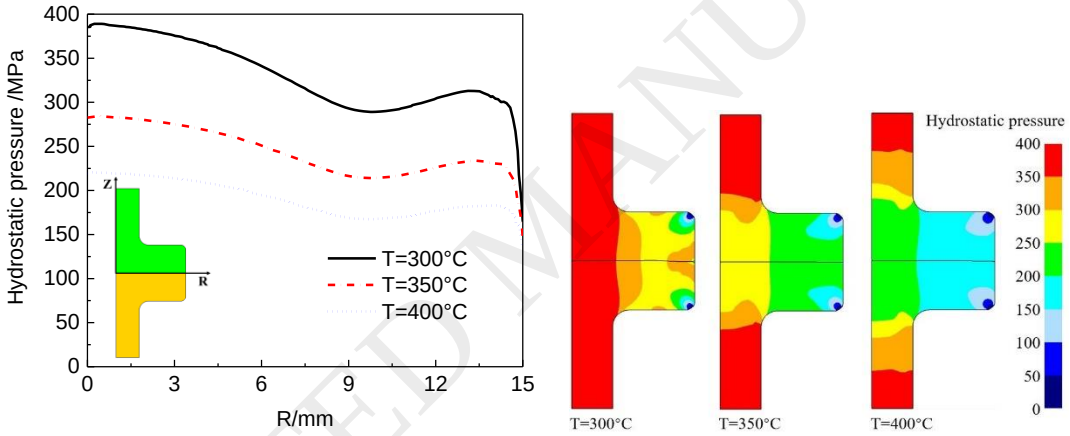

(a) (b)

Fig. 12 FE calculated hydrostatic pressure distributions in the samples extruded at an extrusion speed of 0.8 mm/s and temperatures of 300, 350, 400 ℃: (a) at the welding interface in the radial direction of the die and (b) in the welded samples.

4.2 Mechanical properties

4.2.1 Mechanical properties at different positions

Fig. 13 (a) shows the tensile stress-strain curves of the tensile specimens A, B, C and D (sampling positions are marked in Fig. 4), which were cut out from samples welded

at an extrusion speed of 0.8 mm/s and an initial temperature of 350 °C. The ultimate tensile strength (UTS) values of specimens A, B, C and D were 289.2, 254.2, 250.8 and 174.9 MPa, respectively, and the elongation values were 15.0%, 14.6%, 13.3% and 6.1%, respectively (Fig. 13 b). By comparison, the UTS and elongation of the as-cast magnesium alloy under investigation were measured to be 193.9 MPa and 9.1%, respectively. Obviously, the mechanical properties (UTSs and elongations) of the tensile specimens A-C were much higher than those of the as-cast magnesium alloy. It was attributed to large plastic deformation that the magnesium alloy underwent during extrusion, when the material evolved from the as-cast state to the as-extruded state, accompanied by the increases in UTS and elongation. In addition, the magnesium alloy rods on both sides of the weld seam at positions A, B and C, where the tensile specimens fractured outside the weld seam regions, were bonded well during the extrusion welding process. Fracture of the tensile specimen outside the weld seam region indicated that the bonding strength was higher than, or at least equal to the strength of the deformed material without weld seam. The tensile specimen D fractured in the weld seam region and its UTS was the lowest, because desired solid-state bonding was not achieved.

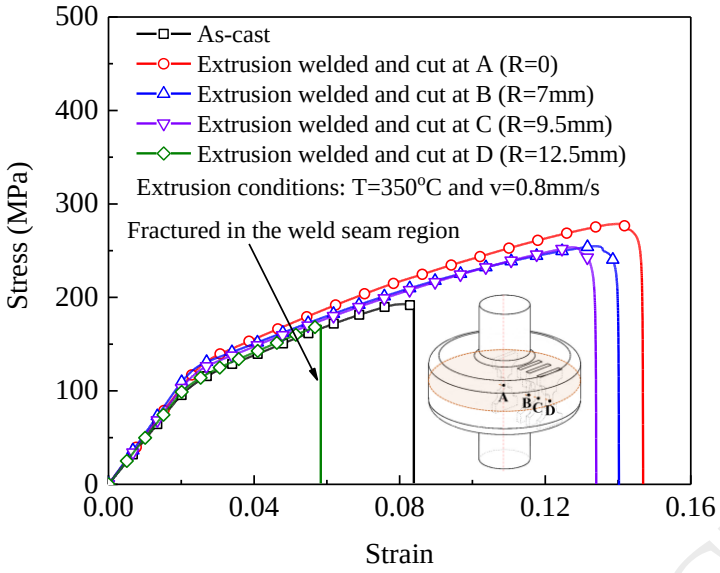

(a)

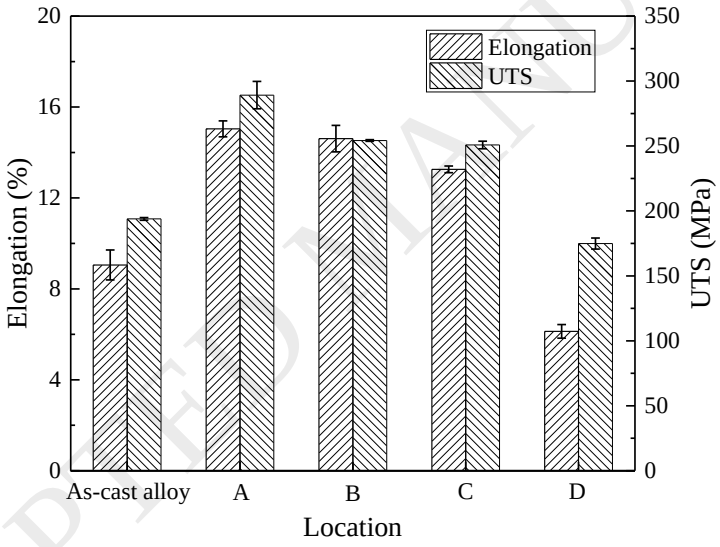

(b)

Fig. 13 Tensile stress-strain curves (a), ultimate tensile strength and elongation values (b) of the specimens cut out from the extrusion-welded samples at positions A (R=0), B (R=7 mm), C (R=9.5 mm) and D (R=12.5 mm).

The solid-state bonding of the magnesium alloy occurred under high hydrostatic pressure inside the welding chamber. It was argued that a higher ratio of hydrostatic pressure P to the equivalent stress σ led to a higher bonding strength (Lu et al.,

2016). The values of P/σ at points A, B, C and D were 5.05, 4.96, 4.48 and 4.55, respectively. Moreover, a high equivalent strain at the welding interface promoted solid-state welding (Bai et al., 2017). The equivalent strains were 4.54, 4.50, 4.79 and 2.54 at points A, B, C and D, respectively (Fig. 7b). As shown in Fig. 13, points A, B and C reached the sound weld seam quality, due to high P/σ values and due to high strains. It seemed that the P/σ value (4.48) at point C was high enough to get a sound weld seam in the current condition. However, point D with a P/σ value (4.55) higher than that of point C had a lower bonding strength (174.9 MPa). It was thus the low strain (2.54) that resulted in the low bonding strength of point D.

4.2.2 Effect of extrusion speed on the mechanical properties of the specimens with weld seam

Three specimens extruded at different speeds and the same initial temperature of 350 °C were cut out at position D (Fig. 4) and the effect of extrusion speed on the mechanical properties of the specimens with weld seam was investigated. Fig. 14 (a) shows the tensile stress-strain curves of three specimens. When the extrusion speeds were 0.8, 1.4 and 2 mm/s, the UTS values were 174.9, 117.5 and 96.2 MPa, respectively, and the elongation values were 6.1%, 3.2% and 2.2%, respectively (Fig. 14 b). The specimens in this group had the UTS and elongation values that were all lower than the values (UTS: 193.9 MPa and elongation: 9.1%) of the as-cast material. It could thus be concluded that the mechanical properties of the magnesium alloy with weld seam decreased with increasing extrusion speed. Moreover, all the tensile specimens in this group fractured in the weld seam region, which indicated that the sound weld seams were not formed at position D under these three conditions.

The influence of extrusion speed on the welding quality is very complex. In general, a high extrusion speed leads to a large value of P/σ, which promotes

solid-state bonding occurring inside the welding chamber. In the present work, when the extrusion speed changed from 0.8 to 1.4 and to 2.0 mm/s, the consequent values of P/σ were 4.55, 4.82 and 4.83, respectively. On the other hand, at given extrusion strokes, welding time is inversely related to extrusion speed. According to the pressure-time criterion proposed by Plata and Piwnik (2000), a long welding time promotes the bonding strength. At extrusion speeds of 0.8, 1.4 and 2.0 mm/s corresponding to the effective welding time values of 105, 60 and 42 s, the material had the bonding strength values of 174.9, 117.5 and 96.2 MPa and elongation values of 6.1%, 3.2% and 2.2%, respectively (Fig. 14). It indicated that a longer welding time led to higher bonding strength and elongation values. Therefore, for this group of welded samples, welding time was another important factor affecting the mechanical properties of the extruded material, in addition to the P/σ value.

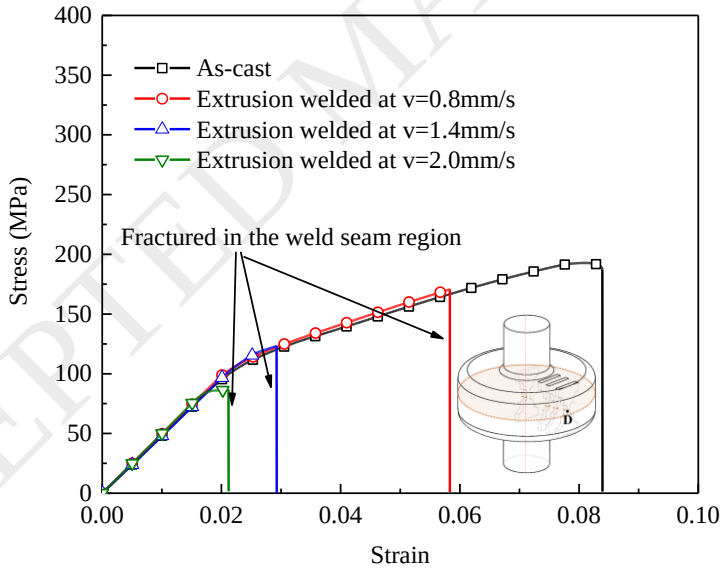

(a)

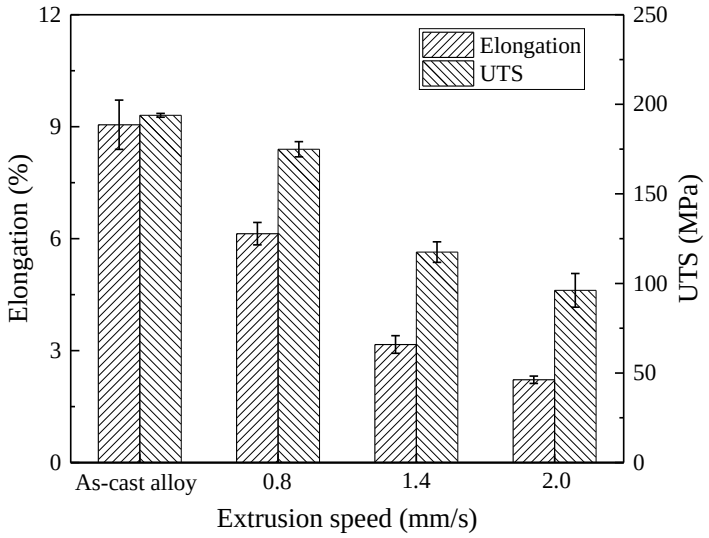

(b)

Fig. 14 Tensile stress-strain curves (a), ultimate tensile strength and elongation values (b) of the specimens cut out from bonded samples at position D (R=12.5 mm), extruded and welded at an initial temperature of 350 °C and extrusion speeds of 0.8, 1.4 and 2 mm/s.

4.2.3 Effect of extrusion temperature on the mechanical properties of the specimens with weld seam

Fig. 15 shows the results of the tensile tests of the specimens extruded at different temperatures and the same extrusion speed of 0.8 mm/s. When the initial temperatures of the rods were 300 and 350 °C, the UTS values of the tensile specimens were 63.2 and 174.9 MPa, respectively, and the elongation values were 1.4% and 6.1%, respectively. As mentioned earlier, the UTS and elongation of the as-cast material were 193.9 MPa and 9.1%, respectively. The mechanical properties of the specimens with weld seam formed at these two temperatures were lower than those of the as-cast alloy. Moreover, the tensile specimens extruded under these two conditions both fractured in the weld seam region. The results indicated that unqualified weld seams appeared at point D at these two extrusion temperatures. When the initial temperature

was increased to 400 °C, however, the measured UTS and elongation values of the specimens increased to 233.3 MPa and 11.0%, respectively. The tensile specimen extruded under this condition fractured outside the weld seam region. Therefore, a sound weld seam was formed at this extrusion temperature. In addition, the mechanical properties of the magnesium alloy with weld seam increased with rising extrusion temperature.

The value of P/σ varied over a range of 4.33, 4.55 and 4.60, when the temperatures were 300, 350 and 400 °C. It was clear that the value of P/σ varying with temperature was a key factor leading to the promotion of bonding strength when the temperature increased. On the other hand, Cooper and Allwood (2014a) proposed that diffusion was an important mechanism in solid-state bonding. High temperature contributes to the diffusion of atoms in the welding region and to void closure at the welding interface (Oosterkamp et al., 2004). Therefore, high temperature plays another important role in improving the weld quality during extrusion welding.

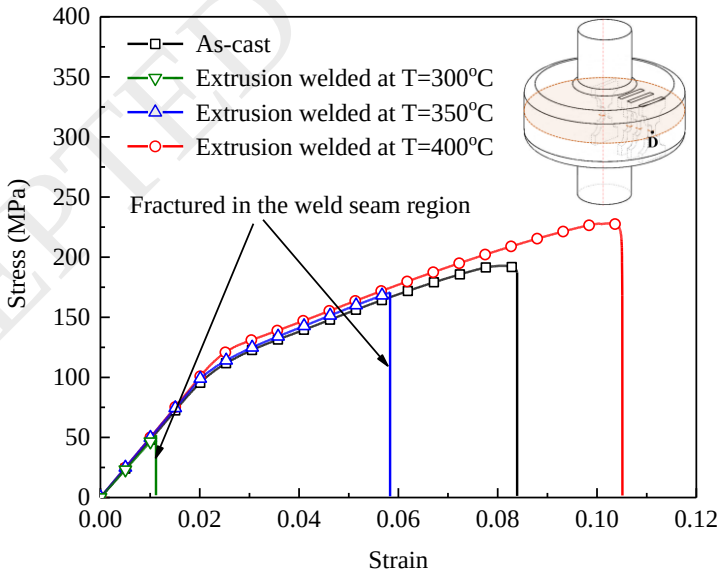

(a)

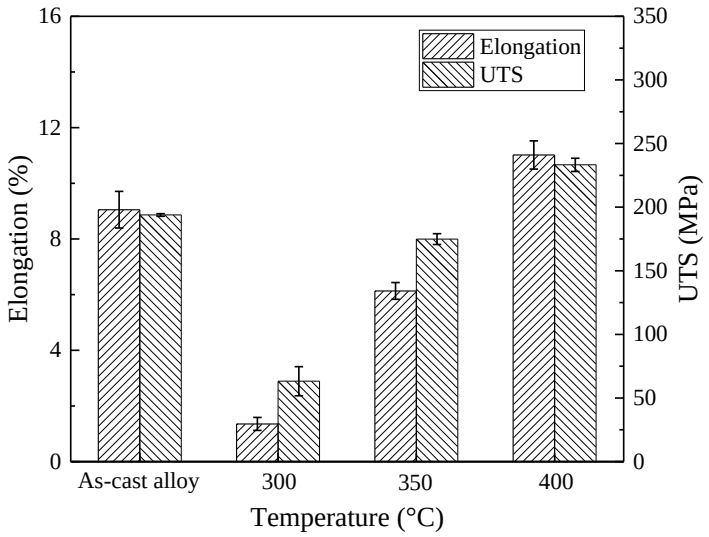

(b)

Fig. 15. Tensile stress-strain curves (a), ultimate tensile strength and elongation values (b) of the specimens cut from bonded samples at location D (R=12.5 mm), extruded and welded at a speed of 0.8 mm/s and different initial temperatures of 300, 350 and 400 °C.

4.3. Microstructure in the welding region

Fig. 16 shows the microstructure of the initial as-cast and solid-solution-treated magnesium alloy Mg-8Al-0.5Zn-0.5RE, which was captured in the polarized light mode. Coarse equiaxed grains were found in the microstructure. The average grain size measured by using the linear intercept method was about 160 μm.

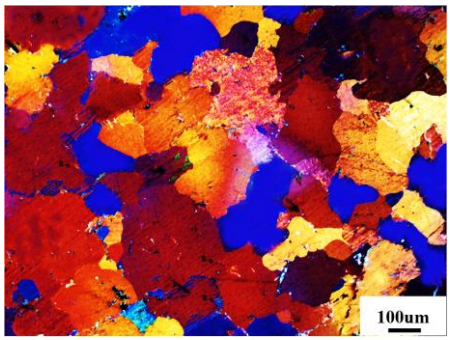

Fig. 16. Optical microstructure of the as-cast alloy solid-solution treated at 420 °C for 24 h.

4.3.1 Microstructures in different zones of extrusion welding

For analyzing the microstructure in different zones nearby the weld seam, the sample extruded at a temperature of 350 °C and speed of 0.8 mm/s was split into two halves. On the longitudinal section, four zones A, B C and D in the bulged part (formed in the welding chamber) of the solid-state bonded rods were selected for microstructure observation, as shown in Fig. 17. These four zones corresponded to the positions of four tensile specimens (Fig. 4). Moreover, the microstructures outside the weld seam region, i.e., the inflowing zone E and the shear concentration zone F were also observed to reveal the flow behavior of the magnesium alloy inside the welding chamber (Fig. 17).

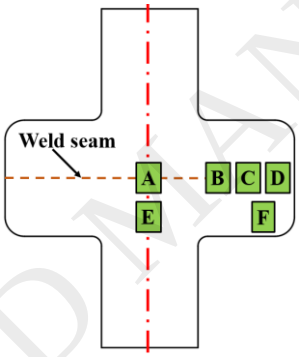

Fig. 17. Six zones in the barreled section of the welded sample for microscopy. A, B, C and D are the welding zones corresponding to the positons of R=0, R=7 mm, R=9.5 mm and R=12 mm, respectively. E is the inflowing zone and F is the shear concentration zone.

Fig. 18a-d shows the microstructures in the welding zones A, B, C and D (as marked in Fig. 17), where the average grain sizes were 9.3, 10.4, 6.9 and 11.1 μm, respectively. Compared with the grain size (about 160 μm) of the as-solution-treated material, the magnesium alloy in the above four zones possessed much finer grains, because it underwent complete dynamic recrystallizations (DRX). FE simulation revealed that the equivalent strains at zones A, B, C and D were 4.54, 4.50, 4.79 and

2.54, respectively (Fig. 7b). Among the four zones, equiaxed grains in zone C were the finest, because the severest deformation occurred there.

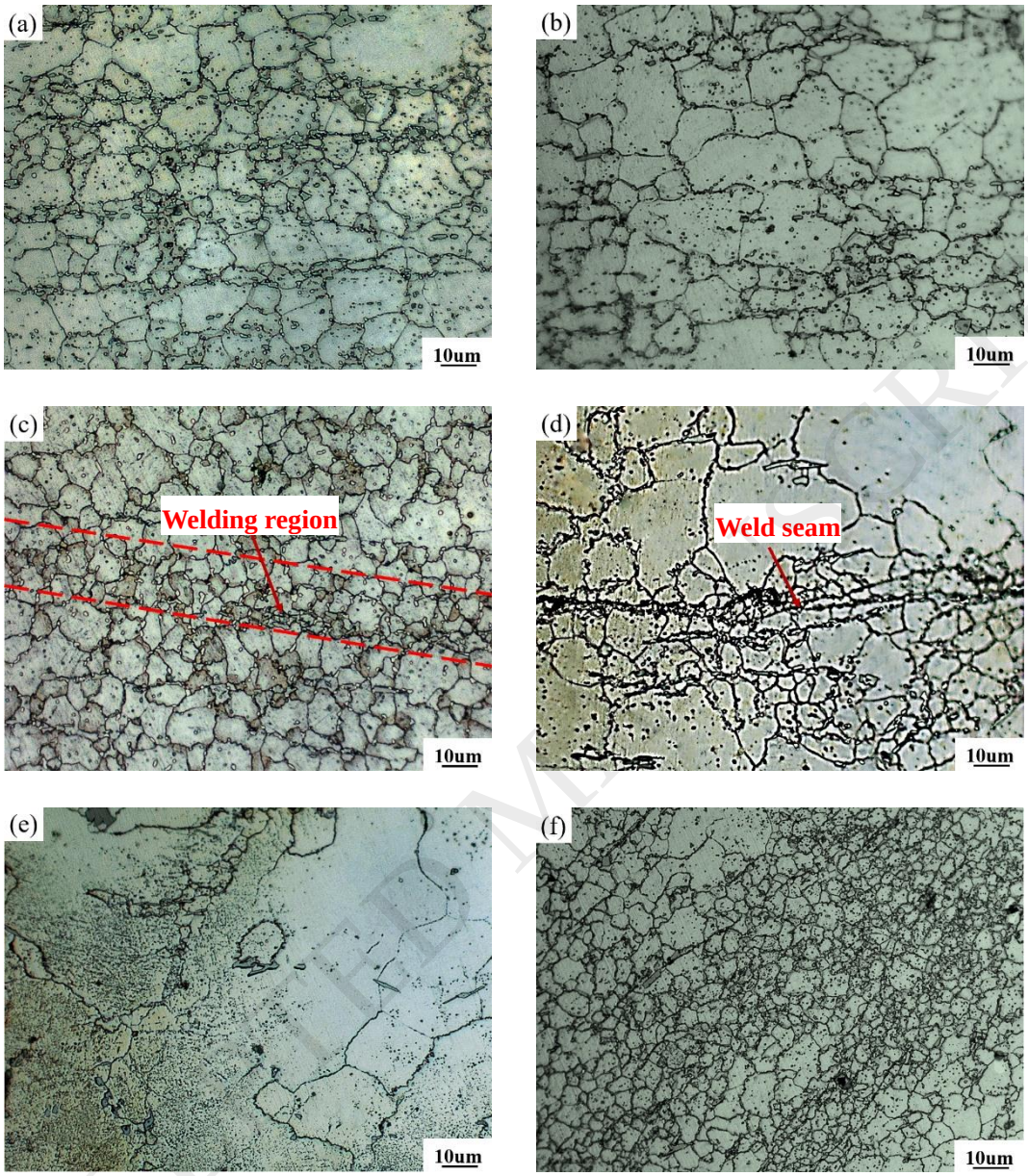

Fig. 18. Microstructures of the extruded material in the welding chamber (sampling zones are shown in Fig. 17). The extrusion condition was: extrusion speed: 0.8 mm/s, initial temperature: 350 °C. (a) welding zone A (R=0), (b) welding zone B (R=7 mm), (c) welding zone C (R=9.5 mm), (d) welding zone D (R=12.5 mm), (e) inflowing zone and (f) shear concentration zone.

In the welding zones A and B, there was no obvious weld seam observable under optical microscope (Fig. 18 a and b), which suggested that sound solid-state bonding was achieved through extrusion welding. This microstructure observation corresponds well to the high bonding strengths of specimens A and B (Fig. 4). Higher bonding strength at point A (289.2 MPa) compared to point B (254.2 MPa) can be explained by the Hall-Petch relationship; strength increases with decreasing grain size. It was not easy to identify the weld seam in the welding region any more, if the magnesium alloy was solid-state bonded well. For other magnesium alloys, Zhang et al. (2017) and Alharthi and Misiolek (2013) found a sound extrusion welding region without obvious weld line. By contrast, in the extrusion welding of aluminum alloys, a weld line was still visible in the bonding region even when sound solid-state bonding was achieved according to bonding strength evaluation (Bai et al., 2017).

There are at least two main reasons for the difference in the visibility of extrusion weld seam between magnesium alloy and aluminum alloy. First, the visible weld line in solid-state bonding is exactly the area with accumulated oxide film and other inclusions. In general, magnesium alloy has a loose and amorphous oxide film, which is easily broken up during extrusion welding under high pressure and at an elevated temperature (You et al., 2000). However, the dense and hard oxide film formed at the bonding interface of aluminum alloy is difficult to break up, resulting in an obvious weld line in the welding region (Cooper and Allwood, 2014b). Secondly, it is easier for DRX to occur in the case of magnesium alloy, because the stacking fault energy of aluminum alloy is higher than that of magnesium alloy (Lin et al., 2013). In the present research, sound solid-state bonding occurred in zones A and B, where fine DRX grains completely occupied the matrix and the weld seam disappeared.

As mentioned above, resulting from a large plastic strain in zone C (Fig. 7 b), the average grain size was 6.9 μm in this zone (Fig. 18 c). The zone C could be recognized under optical microscope (red line in Fig. 18 c), where some fine grains and other inclusions were accumulated. The fine grains resulted in a relatively high bonding strength (250.8 MPa) of the material in this region (Fig. 13).

In zone D, a distinguishable weld seam could be observed under optical microscope, as shown in Fig. 18d. The low equivalent strain (2.54) at point D was the main factor causing unsound solid-state bonding.

Fig. 18e shows the microstructure in the inflowing zone E, where the heterogeneity of grain sizes was a typical feature of incomplete DRX. This was due to a small strain (0.13) in zone E (Fig. 7 b). By contrast, zone F had a higher strain (2.51) and the friction between the magnesium alloy rods and the inner wall of the welding chamber facilitated complete DRX to occur (Fig. 18f).

4.3.2 Microstructures formed at different extrusion speeds

Fig. 19 shows the microstructures in zone D of the samples welded at the same initial temperature of 350 °C and speeds of 0.8, 1.4 and 2.0 mm/s. When the extrusion speeds were 0.8 and 1.4 mm/s, sound weld seams were completely formed (Figs. 19a and b). However, when the extrusion speed increased to 2.0 mm/s, sound weld seam was not formed and voids were present in the welding region, due to a relatively short welding time. Diffusion was the main mechanism of void closure at the weld seam during solid-state bonding. A high extrusion speed corresponded to a short welding time, and a low extent of diffusion between the metal on both sides of the weld seam. As a result, the tensile specimens cut out from zone D extruded at a speed of 2 mm/s had a low UTS value of 96.2 MPa (Fig. 14).

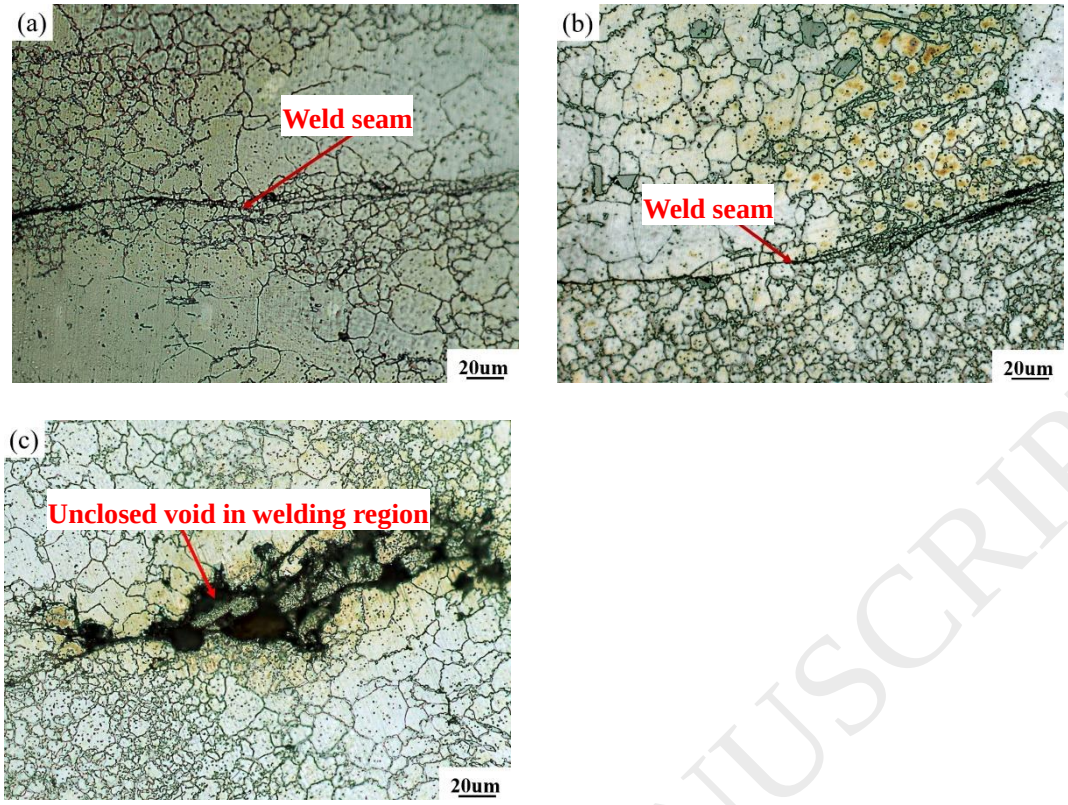

Fig. 19. Microstructures in welding zone D (R=12.5 mm) of welded samples extruded at an initial temperature of 350 °C and speeds of (a) 0.8, (b) 1.4 and (c) 2 mm/s.

4.3.3 Microstructures deformed at different extrusion temperatures

For comparing the microstructures formed at different extrusion temperatures, samples were cut in zone D of the welding region. They were extruded at initial temperatures of 300, 350 and 400 °C and the same speed of 0.8 mm/s. When the initial temperature was 300 °C, the average grain size was less than 3 μm (Fig. 20 a). When the initial temperatures were raised to 350 and 400 °C, the average grain sizes increased to 11.1 and 20.8 μm (Fig. 20b and c), respectively. Li et al. (2014) also concluded that the average size of DRX grains in the ZK60 magnesium alloy increased with rising temperature.

When the initial temperature was 300 °C, sound weld seam in welding zone D was not formed completely (Fig. 20 a), resulting in a low bonding strength of 63.2

MPa (Fig. 15). When the temperatures was increased to 350 and 400 °C, sound weld seams were completely formed but still recognizable in the microstructure. It indicated that a high temperature promoted the closure of voids in the welding region. At a high temperature, the metal on both sides of the interface had a high diffusion rate (Jafarian et al., 2015), which improved the intimacy of contact at the welding interface (Oosterkamp et al., 2004).

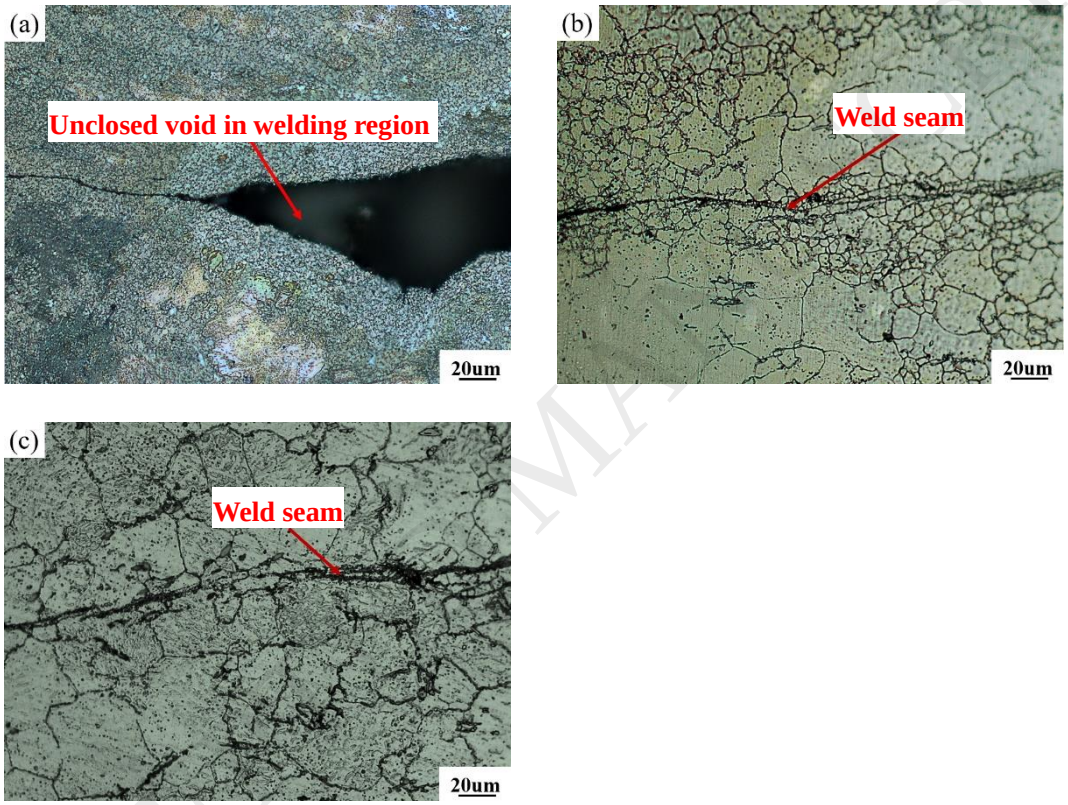

Fig. 20. Microstructures in welding zone D (R=12.5 mm) of the welded samples extruded at a speed of 0.8 mm/s and initial temperatures of (a) 300, (b) 350 and (c) 400 °C.

5. Conclusions

A novel die set-up used to imitate the metal flow inside the welding chamber during real extrusion to produce hollow profiles was developed to investigate the extrusion

welding of the magnesium alloy Mg-8Al-0.5Zn-0.5RE by using the physical simulation method. FE simulations of extrusion welding under the same conditions as those applied in the physical simulation experiments were conducted and the calculated mechanical variables were used in the analysis of extrusion welding. The results obtained from the evaluation of the mechanical properties and from the microstructure observation of the solid-state bonded samples showed that the mechanical properties of the specimens with weld seam and average gain size in the welding region were influenced by the position, extrusion temperature and extrusion speed. The following conclusions were drawn.

(1) With the developed die set-up, extrusion welding could be realized during the physical simulation experiments and the factors influencing the bonding strength and microstructures of the welded magnesium alloy could be investigated separately. With the aid of FE simulation, extrusion welding could be quantitatively analyzed.

(2) Sound weld seams in the center of the welding chamber were obtained, while the magnesium alloy in the marginal space of the welding chamber was insufficiently bonded due to a smaller value of P/σ and a lower strain, compared to the zones close to the center of the welding chamber. The bonding strength decreased with increasing distance from the center of the welding chamber.

(3) High temperature improved the bonding strength, while high extrusion speed decreased the bonding strength. Both low extrusion speed and high temperature contributed to the closure of clearances and voids at the welding interface of two metal streams. Diffusion rate of atoms on both sides of the weld seam was enhanced at elevated temperatures and the extent of diffusion was promoted by increasing welding time when extrusion speed decreased.

(4) When the magnesium alloy was solid-state bonded well enough, the weld seam was unrecognizable under optical microscope. However, poor-quality extrusion welding led to a declined bonding strength. It could even happen that the clearances between the two rods were not closed due to insufficient hydrostatic pressure, welding time and temperature.

(5) Complete DRX occurred and fine grains appeared in the welding region during the physical simulation experiments of the magnesium alloy. The average size of DRX grains increased significantly with rising initial temperature. The visibility of weld seam depended on the local temperature, strain and welding time.

Acknowledgements

The authors (Gang Fang and Sheng-Wen Bai) greatly appreciate the financial support of the National Natural Science Foundation of China (Project No.51675300).

Declarations of interest: none

References

Alharthi, N. H., Misiolek, W. Z., 2013. Microstructure characterization of extrusion welding in a magnesium alloy extrudate. Metallogr. Microstruct. Anal. 2, 395-398.

Alharthi, N., Bingöl, S., Ventura, A., Misiolek, W., 2014. Analysis of extrusion welding in magnesium alloys–numerical predictions and metallurgical verification. Procedia. Eng. 81, 658-663.

Bai, S., Fang, G., Zhou, J., 2017. Analysis of the bonding strength and microstructure of AA6082 extrusion weld seams formed during physical simulation. J. Mater. Process. Technol. 250. 109-120.

Bariani, P., Bruschi, S., Ghiotti, A., 2006 Physical simulation of longitudinal welding in porthole-die extrusion. CIRP. Ann. Manuf. Technol. 55, 287-290.

Cooper, D. R., Allwood, J. M., 2014. Influence of diffusion mechanisms in aluminium solid-state welding processes. Procedia. Eng. 81, 2147-2152.

Cooper, D. R., Allwood, J. M., 2014. The influence of deformation conditions in solid-state aluminium welding processes on the resulting weld strength. J. Mater. Process. Technol. 214, 2576-2592.

Donati, L., Tomesani, L., 2004. The prediction of seam welds quality in aluminum extrusion. J. Mater. Process. Technol. 153, 366-373.

Ebrahimi, G. R., Maldar, A. R., Ebrahimi, R., Davoodi, A., 2011. Effect of thermomechanical parameters on dynamically recrystallized grain size of AZ91 magnesium alloy. J. Alloy. Compd. 509, 2703-2708.

Edwards, S. P., den Bakker, A. J., Zhou, J., Katgerman, L., 2006. Physical simulation of longitudinal weld seam formation in aluminium extrusions. Mater. Sci. Forum. 519, 1403-1408.

Edwards, S. P., Den BAKKER, A. J., Neijenhuis, J. L., Kool, W. H., Katgerman, L., 2006. The influence of the solid-state bonding process on the mechanical integrity of longitudinal weld seams. JSME. Int. J. Ser. A 49, 63-68.

Fang, G., Nguyen, D-T., Zhou, J., 2017. Physical simulation method for the investigation of weld seam formation during the extrusion of aluminum alloys. JOM. 69, 734-741.

Gensch, F., Gall, S., Fahrenson, C., Müller, S., Reimers, W., 2016. Characterization of weld seam properties of extruded magnesium hollow profiles. J. Mater. Sci. 51, 3888-3896.

Jafarian, M., Khodabandeh, A., Manafi, S., 2015. Evaluation of diffusion welding of 6061 aluminum and AZ31 magnesium alloys without using an interlayer. Mater. Des. 65, 160-164.

Khan, Y. A., Valber, H. S., 2010. Metal flow in idealised a-symmetric 2D extrusion welding. Int. J. Mater. Form. 3, 383-386.

Khan, Y. A., Khorasani, S. T., Valberg, H. S., 2012. Analysis of gas pocket formation during extrusion of Al hollow profiles and establishing an extrusion seam weld limit diagram. Key. Eng. Mater. 491, 197-204.

Lee, J. M., Kim, B. M., Kang, C. G., 2005. Effects of chamber shapes of porthole die on elastic deformation and extrusion process in condenser tube extrusion. Mater. Des. 26, 327-336.

Letzig, D., Swiostek, J., Bohlen, J., Beaven, P., Kainer, K., 2008. Wrought magnesium alloys for structural applications. Mater. Sci. Technol. 24, 991-996.

Li, J., Liu, J., Cui, Z., 2014. Characterization of hot deformation behavior of extruded ZK60 magnesium alloy using 3D processing maps. Mater. Des. 56, 889-897.

Li, L., Zhang, H., Zhou, J., Duszczyk, J., Li, G., Zhong, Z., 2008. Numerical and experimental study on the extrusion through a porthole die to produce a hollow magnesium profile with longitudinal weld seams. Mater. Des. 29, 1190-1198.

Lin, Y., Ding, Y., Chen, M-S., Deng, J., 2013. A new phenomenological constitutive model for hot tensile deformation behaviors of a typical Al–Cu–Mg alloy. Mater. Des. 52, 118-127.

Liu, G., Zhou, J., Duszczyk, J., 2008. FE analysis of metal flow and weld seam formation in a porthole die during the extrusion of a magnesium alloy into a square tube and the effect of ram speed on weld strength. J. Mater. Process. Technol. 200, 185-198.

Liu, Z., Li, L., Yi, J., Li, S., Wang, G., 2017. Influence of extrusion speed on the seam weld quality in the porthole die extrusion of AZ31 magnesium alloy tube. Int. J. Adv. Manuf. Technol. 92, 1039-1052.

Lu, X., Zhang, C., Zhao, G., Guan, Y., Chen, L., Gao, A., 2016. State-of-the-art of extrusion welding and proposal of a method to evaluate quantitatively welding quality during three-dimensional extrusion process. Mater. Des. 89, 737-748.

Oosterkamp, A., Oosterkamp, L. D., 2004. "Kissing bond" phenomena in solid-state welds of aluminum alloys. Weld. J. 83, 225-231.

Plata, M., Piwnik, J., 2000. Theoretical and experimental analysis of seam weld formation in hot extrusion of aluminum alloys. In: Proceedings of the Seventh International Aluminum Extrusion Technology Seminar, Chicago, Illinois USA. pp. 205-211.

Quan, G. Z., Ku, T. W., Song, W. J., 2011. Kang B S. The workability evaluation of wrought AZ80 magnesium alloy in hot compression. Mater. Des. 32, 2462-2468.

Tang, D., Fang, W., Fan, X., Li, D., Peng, Y., 2014. Effect of die design in microchannel tube extrusion. Procedia. Eng. 81, 628-633.

Tang, D., Zhang, Q., Li, D., Peng, Y., 2014. A physical simulation of longitudinal seam welding in micro channel tube extrusion. J. Mater. Process. Technol. 214, 2777-2783.

You, B-S., Park, W-W., Chung, I-S., 2000. The effect of calcium additions on the oxidation behavior in magnesium alloys. Scripta. Mater. 42, 1089-1094.

Yu, J., Zhao, G., Chen, L., 2016. Analysis of longitudinal weld seam defects and investigation of solid-state bonding criteria in porthole die extrusion process of aluminum alloy profiles. J. Mater. Process. Technol. 237, 31-47.

Yu, J., Zhao, G., Chen, L., 2016. Investigation of interface evolution, microstructure and mechanical properties of solid-state bonding seams in hot extrusion process of aluminum alloy profiles. J. Mater. Process. Technol. 230, 153-166.

Yu, J, Zhao, G., Cui, W., Zhang, C., Chen, L., 2017. Microstructural evolution and mechanical properties of welding seams in aluminum alloy profiles extruded by a porthole die under different billet heating temperatures and extrusion speeds. J. Mater. Process. Technol. 247, 214-222.

Zhang, J., Chen, L., Zhao, G., Zhang, C., Zhou, J., 2017. Study on solid bonding behavior of AZ31 Mg alloy during porthole die extrusion process. Int. J. Adv. Manuf. Technol. 93, 2791-2799.

Table Captions

Figure Captions

Fig. 8. Extrusion-welded sample at a punch stroke of 42 mm, an extrusion speed of 0.8 mm/s and a temperature of 350 °C.

Fig. 9 Temperature evolution at a point monitored by a thermocouple during extrusion welding at an initial temperature of 350 °C and extrusion speeds of 0.8, 1.4 and 2 mm/s.

Fig. 10 Distribution of hydrostatic pressures at the welding interface during extrusion welding at an extrusion speed of 0.8 mm/s and a temperature of 350 °C.

Fig. 11. FE calculated hydrostatic pressure distributions in the samples extruded at an initial temperature of 350 °C and speeds of 0.8, 1.4, 2.0 mm/s: (a) at the welding interface in the radial direction of the die and (b) in the welded samples.

Fig. 12 FE calculated hydrostatic pressure distributions in the samples extruded at an extrusion speed of 0.8 mm/s and temperatures of 300, 350, 400 °C: (a) at the welding interface in the radial direction of the die and (b) in the welded samples.

Fig. 13 Tensile stress-strain curves (a), ultimate tensile strength and elongation values (b) of the specimens cut out from the extrusion-welded samples at positions A (R=0), B (R=7 mm), C (R=9.5 mm) and D (R=12.5 mm).

Fig. 14 Tensile stress-strain curves (a), ultimate tensile strength and elongation values (b) of the specimens cut out from bonded samples at position D (R=12.5 mm), extruded and welded at an initial temperature of 350 °C and extrusion speeds of 0.8, 1.4 and 2 mm/s.

Fig. 15. Tensile stress-strain curves (a), ultimate tensile strengths and elongations (b) of specimens located at D (R=12.5 mm) welded at a speed of 0.8 mm/s and different initial temperatures of 300, 350 and 400 °C, and the extrusion speed (stem) is 0.8 mm/s and the samples were cut from the position at D (R=12.5 mm).

Fig. 16. Optical microstructure of the as-cast alloy solid-solution treated at 420 °C for 24 h.

Fig. 17. Six zones in the barreled section of the welded sample for microscopy. A, B, C and D are the welding zones corresponding to the positons of R=0, R=7 mm, R=9.5 mm and R=12 mm, respectively. E is the inflowing zone and F is the shear concentration zone.

Fig. 18. Microstructures of the extruded material in the welding chamber (sampling zones are shown in Fig. 17). The extrusion condition was: extrusion speed: 0.8 mm/s, initial temperature: 350 °C. (a) welding zone A (R=0), (b) welding zone B (R=7 mm), (c) welding zone C (R=9.5 mm), (d) welding zone D (R=12.5 mm), (e) inflowing zone and (f) shear concentration zone.

Fig. 19. Microstructures in welding zone D (R=12.5 mm) of welded samples extruded at an initial temperature of 350 °C and speeds of (a) 0.8, (b) 1.4 and (c) 2 mm/s.

Fig. 20. Microstructures in welding zone D (R=12.5 mm) of the welded samples extruded at a speed of 0.8 mm/s and initial temperatures of (a) 300, (b) 350 and (c) 400 °C.